Computed diffusion weighted imaging (cDWI) and voxelwise-computed diffusion weighted imaging (vcDWI) for oncologic liver imaging: A pilot study

Ferdinand Seith[a,*], Petros Martirosian[b], Konstantin Nikolaou[a], Christian la Fougère[c], Nina Schwenzer[a], Holger Schmidt[a]

[a] *Diagnostic and Interventional Radiology, University Department of Radiology, University Hospital of Tuebingen, Hoppe-Seyler-Str. 3, 72076 Tuebingen, Germany*
[b] *Section on Experimental Radiology, Diagnostic and Interventional Radiology, University Department of Radiology, University Hospital of Tuebingen, Hoppe-Seyler-Str. 3, 72076 Tuebingen, Germany*
[c] *Nuclear Medicine and Clinical Molecular Imaging, Department of Radiology, University Hospital of Tuebingen, Otfried-Mueller-Strasse 14, 72076 Tuebingen, Germany*

A B S T R A C T

Objective: Aim of the study was to evaluate the influence of the selection of measured b-values on the precision of cDWI in the upper abdomen as well as on the lesion contrast of PET-positive liver metastases in cDWI and vcDWI.
Methods: We performed a retrospective analysis of 10 patients (4 m, 63.5 ± 12.9 y/o) with PET-positive liver metastases examined in 3 T-PET/MRI with b = 100,600,800,1000 and 1500s/mm^2. cDWI (cb1000/cb1500) and vcDWI were computed based on following combinations: i) b = 100/600 s/mm^2, ii) b = 100/800 s/mm^2, iii) b = 100/1000s/mm^2, iv) b = 100/600/1000s/mm^2 v) all measured b-values. Mean signal intensity (SI) and standard deviation (SD) in the liver, spleen, kidney, bone marrow and in liver lesions were acquired. The coefficient of variation (CV = SD/SI), the differences of SI between measured and calculated high b-value images and the lesion contrast (SI lesion/liver) were computed.
Results: With increasing upper measured b-values, the CV in cDWI and vcDWI decreased (CV in the liver in cb1500: 0.42 with b100/600 s/mm^2 and 0.28 with b100/b1000s/mm^2) while the differences of measured and calculated b-value images decreased (in the liver in cb1500: 30.7% with b = 100/600 s/mm^2, 19.7% with b100/b1000s/mm^2). In diffusion-restricted lesions, lesion contrast was at least 1.6 in cb1000 and 1.4 in cb1500, respectively, with an upper measured b-value of b = 800 s/mm^2 and 2.1 for vcDWI with an upper measured b-value of b = 1000s/mm^2. Overall, the lesion contrast was superior in cb1500 and vcDWI compared to cb1000 (15% and 11%, respectively).
Conclusion: Measuring higher upper b-values seems to lead to more precise computed high b-value images and a decrease of CV. vcDWI provides a comparable lesion contrast to b = 1500s/mm^2 and offers additionally the reduction of T2 shine-through effects. For vcDWI, measuring b = 1000s/mm^2 as upper b-value seems to be necessary to guarantee good lesion visibility in the liver based on our preliminary results.

1. Introduction

Diffusion-weighted imaging (DWI) has become one of the most widely used functional imaging techniques in magnetic resonance imaging (MRI). Within a few minutes, DWI is able to provide tissue information on a molecular scale [1]. Technical developments such as the introduction of single shot echo planar imaging (EPI) and parallel imaging improved image quality and allowed for the application of DWI in extracranial regions [2,3]. While malignant tumors usually show different tissue characteristics to the tissue they arise from (such as higher cellularity or the integrity of cell membranes), DWI nowadays plays a pivotal role in oncologic abdominal imaging [4,5]. Technically, DWI is based on a T2-weighted spin-echo EPI sequence modified by diffusion-sensitizing paired gradients [6]. The sensitivity can be varied

by the time interval between the gradients, the duration and the amplitude of the applied gradients which is subsumed under the term "b-value". As DWI is based on a T2-weighted sequence, the signal intensity in b-value images does not only depend on the diffusivity of water molecules but also on the T2 relaxation properties of the investigated tissue. This is known as T2 shine-through effect and might result in misleading interpretations. It has been shown that high b-value images of up to b = 1000–1500 s/mm^2 can improve tumor detection in selected anatomic sites [7,8]. As acquiring high b-value images can time consuming and more prone to image artifacts as compared to lower b-value images, they have not been implemented in daily routine of whole-body imaging so far [9,10]. With the aim to improve image quality, Blackledge et al. proposed an approach to compute high b-value images based on lower measured b-value images: computed DWI

(cDWI) [11]. This has mostly been evaluated in the prostate [9,10,12,13]. However, the precision of computed high b-value images and the dependence on measured lower b-value images have not been investigated yet in the upper abdomen. Recently, Gatidis et al. proposed a new voxelwise computed DWI (vcDWI) technique to further improve the visibility of diffusion restricted lesions [14]. In contrast to the method by Blackledge et al., it computes the presented b-value image for each voxel in dependence on its apparent diffusion coefficient (ADC) and calculates its respective intensity value. Thereby, voxels with low ADC are presented with signal intensity of low b-values and vice versa. This should improve the contrast of diffusion restricted lesions and reduce the T2 shine-through effect.

The aim of our study was twofold: First, to investigate the influence of the selection of measured b-value images on the precision of computed high b-value images (cDWI) in the upper abdomen. Second, to evaluate quantitative image features of cDWI and vcDWI in organs and metastatic liver lesions in dependence on the measured b-value images used for the computation.

2. Material and methods

2.1. Patient cohort

The data of 10 consecutive patients (4 male, mean age 63.5 ± 12.9 years) with PET-positive liver metastases and a PET/MRI protocol including DWI with high b-value images (up to b = 1500s/mm^2) were retrospectively evaluated. The local ethics committee waived informed consent for the retrospective evaluation of the data. The oncologic diseases were distributed as follows: Melanoma (n = 5), neuroendocrine tumor (n = 3), adenocarcinoma of the small bowel (n = 1), breast cancer (n = 1). Metastatic involvement of the liver was histology-proven in four patients. In six patients, follow-up examinations revealed progressive metastatic disease of the liver (n = 5) or response under therapy (n = 1).

2.2. PET/MRI protocol

All patients were examined in a simultaneous 3 T PET/MRI-scanner (Biograph mMR, Siemens Healthcare GmbH, Erlangen, Germany). A 2D single-shot spin-echo EPI sequence in 3-scan-trace mode with monopolar diffusion gradients and five different b-values (b = 100, 600, 800, 1000 and 1500s/mm^2) was applied in the upper abdomen of each patient. Sequence parameters are given in Table 1. Additionally, a navigator-triggered T2-weighted 3D fast-spin-echo sequence (T2-TSE) was performed. Other sequences were chosen depending on clinical indication. Depending on the disease, ^{18}F-FDG (melanoma, adenocarcinoma, breast cancer) or ^{68}Ga-DOMITATE (neuroendocrine tumor) was used as PET-tracer.

Table 1
Sequence parameters of DWI. Examinations were performed in free breathing.

	DWI
Echo Time	65 ms
Repetition Time	7300 ms
Matrix Size	168 × 192
Pixel Size	2.2 x 2.2 mm
Slice Thickness	5 mm
Number of slices	34
Pixel Bandwidth	1736 Hz/pixel
Acquisition Time	2.5 min
Field of view	350 × 400
Number of averages	5
Acquisition plane	axial
b-values (s/mm^2)	100, 600, 800, 1000, 1500
Fat suppression method	Spectral attenuated inversion recovery fat suppression

2.3. The computation of cDWI/vcDWI

While in the cDWI method the signal intensity of each image voxel is calculated for a predefined constant b-value [11], in the vcDWI method the chosen b-value for each voxel varies dependent on its ADC-value: $S_b(x) = S_0(x) * exp(-ADC(x) * (k*ADC(x)-b_0))$, where $S_b(x)$ is the calculated signal intensity of voxel x for a b-value (k*ADC(x)), S0(x) its measured signal intensity with b-value = 0 s/mm^2 (b$_0$), ADC(x) is its ADC value and k = 10^6 s^2/mm^4. The ADC-dependent choice of the voxelwise-computed b-value can thus increase the contrast between diffusion-restricted and unrestricted tissues because signal intensities of voxels with low ADC are computed at lower b-values while voxels with high ADC at higher b-values [14].

VcDWI as well as cDWI images for b = 1000 and b = 1500s/mm^2 (cb1000 and cb1500, respectively) were calculated based on a mono-exponential model from five different combinations of b-value images: i) b = 100 and 600 s/mm^2 (b100/600), ii) b = 100 and 800 s/mm^2 (b100/800), iii) b = 100 and 1000s/mm^2 (b100/1000), iv) b = 100, 600 and 1000s/mm^2 (b100/600/1000) v) all measured b-value images (b_all). The calculation of cDWI and vcDWI was carried out as described in Blackledge et al. [11] and the recently published work by Gatidis et al. [14] using MATLAB (The MathWorks Inc, Natick, MA).

2.4. Image analysis

To avoid partial volume effects, only lesions with a diameter of > 1 cm were included to the quantitative evaluation. Lesions were rated as PET-positive if the focal tracer uptake exceeded the regional uptake of physiological liver tissue. For anatomical correlation, the T2-TSE images were rigidly registered to the b = 800 images. Regions of interest (ROIs) were drawn freehand in the b = 800 images in up to three PET-positive lesions of the liver by F.S. (6 years of experience in MRI, 4 years of experience in hybrid imaging). Furthermore, circular ROIs were set in visually not affected parenchyma of the right and left liver lobe, the spleen, the right or left kidney, the psoas muscle, the second lumbar vertebra (bone marrow) and the image background. Care was taken to avoid image artifacts and borders of organs and lesions. ROIs in physiological tissue and background had a target diameter of 1.5 cm in the liver and 1 cm in other organs. The ROIs were copied to the different measured and computed b-value images. Those steps were performed using PMod (PMOD Technologies Ltd, Zurich, Switzerland). Mean signal intensities (SI) were measured in each ROI. Standard deviations (SD) were acquired in tissue ROIs in cDWI and vcDWI. SI of the liver was defined as the mean value of SI in the right and left liver lobe. Measured b = 1000s/mm^2 and b = 1500s/mm^2 images are abbreviated as "mb1000" or "mb1500" in the following, respectively.

The following parameters were calculated:

The relative signal difference of physiological tissue ROIs between the measured and calculated (cDWI) b-value images:

Relative differences = abs (SI calculated b-value image – SI measured b-value image) / SI measured b-value image * 100.

The contrast (signal intensity ratio) of the lesion ROIs to the surrounding liver tissue (liver ROI) for the different measured b-value images as well as for cDWI and vcDWI:

Lesion contrast = lesion SI / liver SI.

The coefficient of variation within the different physiological tissue ROIs for the different measured b-value images as well as for cDWI and vcDWI as an indicator of the image noise:

CV = SD / SI.
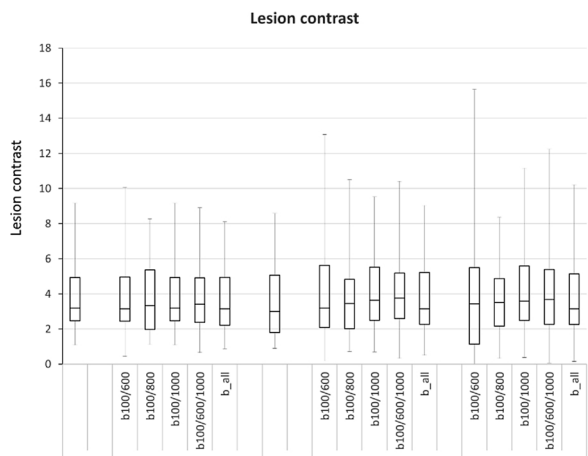
Lesion contrast

Fig. 1. Whisker box plots including median, first and third quartile, maximum and minimum of lesion contrast of measured and calculated b-values as well as in vcDWI. The mean lesion contrasts of cb1500 and vcDWI seem to be on a comparable level. However, highest variances in computed b-value images as well as in vcDWI are seen with b = 100/600, resulting in values partially close to zero.

3. Results

In total, 20 liver metastases (in 10 patients) with diameters ranging from 1.0 to 4.8 cm were evaluated. The SI, the relative differences between measured and calculated b-value images, the CV and the lesion contrast are shown in Figs. 1–4 respectively.

The SI in physiological tissue and lesions in mb1500 images were about 39% lower than in mb1000 images. For cDWI, SI in physiological tissues showed to be relatively stable and rather independent on the measured b-values used for calculation (max. 23% difference for cb1000 in lesions between b100/600 and b100/1000). VcDWI provided SI approximately on the level of b = 1000 images with highest SI for b100/1000 calculations, especially in lesions (Fig. 2). In the spleen, as an organ with inherently low diffusivity, vcDWI provided higher SI as compared to all other measured and calculated images. However, an overall higher dependence of lesion SI on b-value selection – especially for lesion ROIs – was found in vcDWI.

While cb1000 images showed only a slight underestimation of mean signal intensities as compared to mb1000 images, a pronounced underestimation was seen in the cb1500 images on average (maximum of

15.7 and 28.3%, respectively, Figs. 2 and 4). With increasing upper measured b-value images, the relative differences between measured and calculated b-value images showed a decreasing trend.

Overall, the CVs of cb1500 images were higher than in cb1000 images (Fig. 3). The CVs in cDWI and vcDWI showed a decreasing trend with increasing upper measured b-value images. However, the CVs in high b-values images calculated with b100/600/1000 were higher than for b100/1000 in the kidney and liver. In vcDWI, the CV was higher in the liver, the kidneys and the muscle as in computed b-value images while it was on a comparable level in the spleen and the bone marrow (CV in the liver when computation was based on b100/800: cb1000, 0.23; cb1500, 0.35; vcDWI, 0.48). In the image background, the CV in vcDWI was lower than in the cb1500 images.

The lesion contrast was slightly superior in cb1500- and vcDWI-images as compared to cb1000-images (maximum 15% and 11%, respectively; Fig. 1). On the other hand, cb1500 and vcDWI images also provided higher variances in lesion contrast; the highest ranges of lesion contrast were found in cDWI and vcDWI when based on b100/600 (min/max: cb1000, 0.4/10.1; cb1500, 0.2/13.1; vcDWI, 0/15.6).

Fig. 5 gives an example of a patient with liver metastases of melanoma to demonstrate the image impression and lesion contrast of the different measured and calculated b-value images as well as the vcDWI. The smaller lesion, marked with a dotted arrow in the Figure, is smaller than 1 cm in diameter and was therefore not included to the quantitative evaluation.

4. Discussion

In this study, we investigated the influence of the selection of measured b-value images on the precision, the image characteristics and the lesion contrast of cDWI and vcDWI approaches in the upper abdomen.

Diffusion-weighted imaging is based on a T2-weighted sequence. Therefore, the signal intensities in images are influenced by both the T2 properties and the diffusion restriction of the investigated tissue. With increasing b-values, the diffusion-weighting increases and thus the SI decreases (especially for less diffusion-restricted tissues). As expected, the mb1500 images consecutively showed lower signal intensities than mb1000 images in our study. The mean signal intensities of computed b-value images seem to be rather stable and independent on the used measured b-value images for calculation. While the computation of cb1000 images was relatively precise, a pronounced underestimation of cb1500 images on average was observed. The computation of high b-
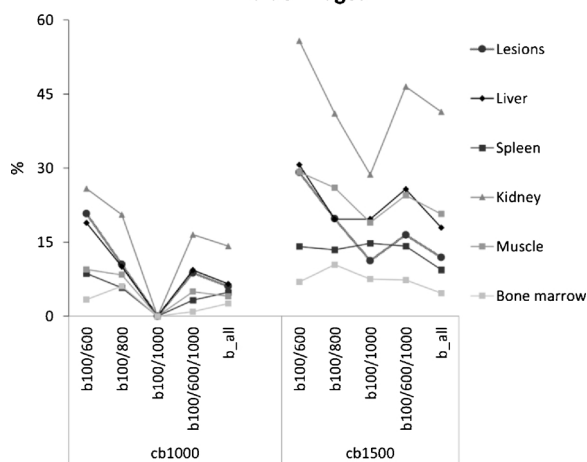
Mean signal intensities
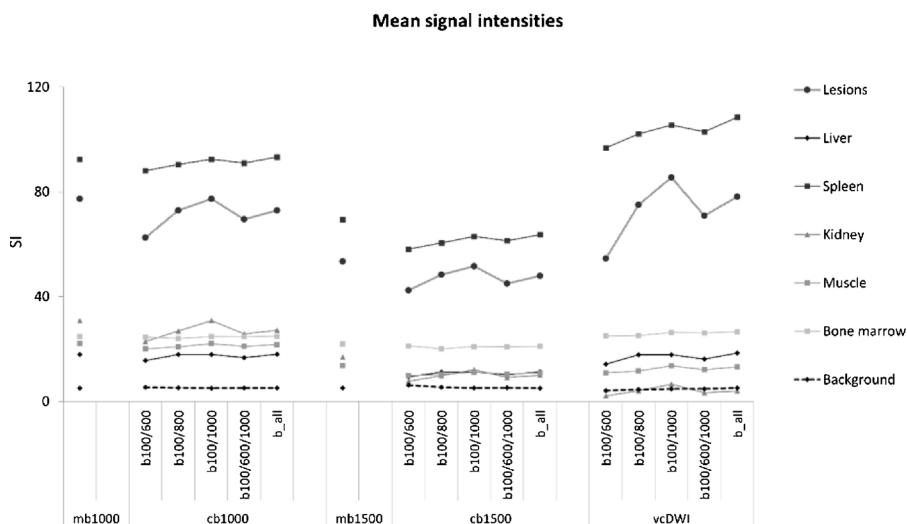
Fig. 2. Mean signal intensities of measured and computed b-values as well as vcDWI in lesions and organs. Note the superior signal intensity in lesions in vcDWI compared to measured and calculated b1500. Physiological spleen tissue also shows high signal intensity caused by high cellularity.

Coefficient of variation
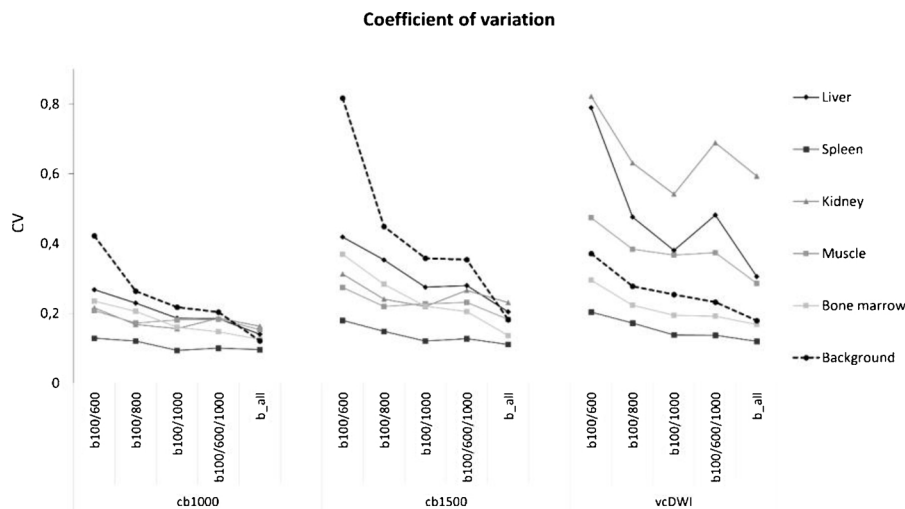
Fig. 3. Coefficient of variation in physiological tissue and image background. Taking higher b-value images for the calculation of cb1000 and cb1500 decreases the covariance. Overall, vcDWI shows higher CV in physiological tissue; the high CV in vcDWI in kidneys and background are mainly caused by the very low signal intensity in those ROIs (see Fig. 2).

Differences between measured and calculated b-value images

Fig. 4. Relative differences of the mean signal intensities between measured and computed b-value images in %. A slight trend towards decreasing deviations with increasing upper b-values is present while b = 100/1000 provides overall best results for most organs in cb1500 from the b-value combinations tested.

value images in our study is based on a mono-exponential fit which is a model assuming free Gaussian diffusion as a normal distribution of tissue diffusivities. However, as shown in several studies, this is only a simplified model which does not reflect the true diffusion properties of human tissue [15–17]. Several approaches have been proposed trying to take these effects into account like bi-exponential models or diffusion kurtosis imaging [18,19]. However, they have not been implemented into daily routine of abdominal DWI so far. The multi-exponential dependence of the diffusion signal on b-value images (or diffusion-weighting) is the main reason for the difference between measured and computed b-value images. If a higher upper b-value is close to the value to be computed, the deviation to the measured value in a mono-exponential fit is expected to be low. Overall, a trend towards lower deviations with higher upper measured b-value images was observed in our study which is in concordance to previously reported results [20]. Using the b = 600 s/mm^2 value to the calculation of cb1500 decreased the precision of calculation in most tissue types in organs with higher perfusion content (liver and kidney). Therefore, from a quantitative point of view b = 600 s/mm^2 seems not to be valid for calculation of high b-value images in those organs.

The differences of measured and calculated b-value images were

highest in the kidneys. A reason might be that the kidneys are organs with a high portion of capillary perfusion and an anisotropic diffusion; therefore it is likely that the b100 value is strongly influenced by perfusion effects [21]. To reduce the influence of these perfusion effects on DWI, previously conducted studies suggest b-values of at least b = 800 s/mm^2 [22]. This can also be seen in our study in a noticeable drop of computed-to-measured deviations from b = 100/600 to b = 100/800 which is synonymous with a more precise ADC measurement.

As the SI in calculated b-value images is relatively stable, the decreasing trend seen in CVs is mainly caused by decreasing standard deviations. As standard deviation represents the inhomogeneity of signal intensities within a ROI, the reason for this behaviour might be found in the more precise voxelwise computation of high b-value images with higher upper b-value images. Therefore, the course of CVs resembles the course of the relative differences between measured and calculated b-value images. For vcDWI, the b-value of each voxel is calculated based on the ADC-measurement. Therefore, deviations in the ADC-map lead to even more pronounced deviations in the vcDWI-images as compared to the calculated high b-value images. This is represented in the higher CVs in physiological tissue. In contrast, the CVs in the image background in vcDWI is relatively low.

In concordance to the behaviour of CV and differences in signal intensities, highest variances in lesion contrast of cb1000, cb1500 and vcDWI occurred if the calculation was based on b100/600. This led to a lesion contrast of < 1 in calculated b-value images in two lesions and in vcDWI in five lesions out of 20. This is crucial as it might result in misinterpretations in oncologic reading. In one of the patients, the investigated ^{68}Ga-PET-positive lesion showed low signal intensities and a lesion contrast below 1 in most calculated b-value images, in mb1500 and even close to zero in vcDWI, respectively. This example is demonstrated in Fig. 6. This patient suffered from a metastasized neuroendocrine tumor and had undergone systemic therapy. As a possible response to therapy it can be seen that metastases change their tissue properties caused by cell swelling, tumor lysis and necrosis [23–26]. Therefore, the diffusivity can increase and the signal intensity in high b-values and vcDWI therefore decrease. The very low lesion contrast in this case is therefore not to be interpreted as an incorrect computation of b-value images or a drawback of vcDWI but as a therapy response and a general limitation in the detection of liver metastases in DWI as DWI is merely able to detect diffusion restricted lesions. Thus, in this case the lesion contrast in measured b-value images was most probably not due to differences in tissue diffusion restriction but because of differences in T2 relaxation times. Since the vcDWI method reduces such effects, this result in the observed loss in lesion liver contrast. This should be kept in mind when using vcDWI. Besides this case, the lesion
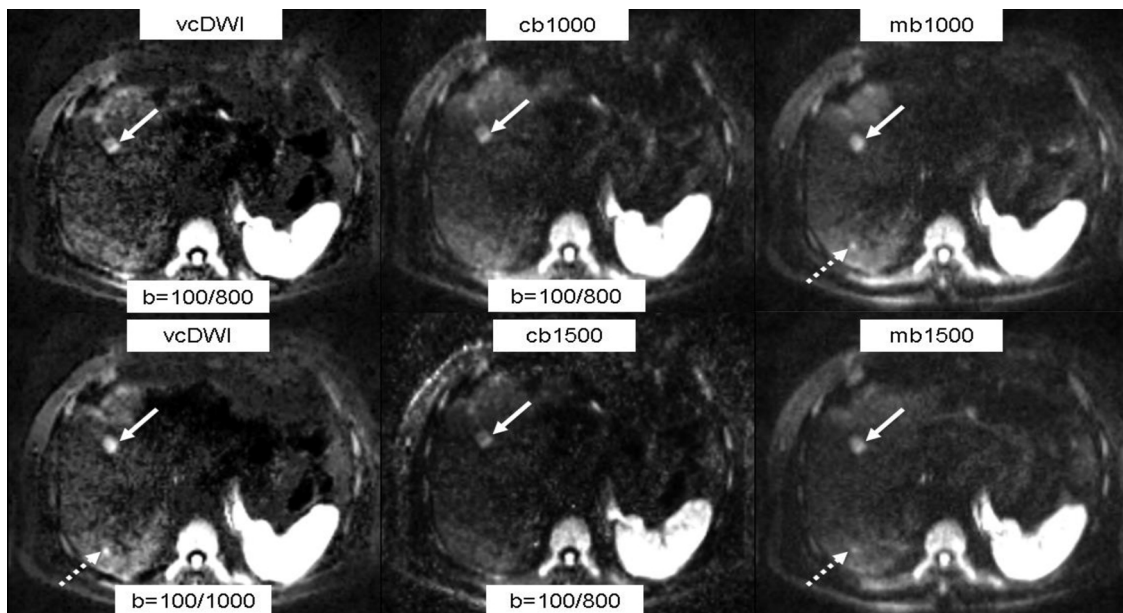
Fig. 5. Example of a 60 y/o male patient with melanoma and metastatic liver lesions. The larger lesion (white arrow) can clearly be seen in vcDWI as well as in computed and measured b-values (cb and mb, respectively); note the differences in lesion-to-liver contrast and image noise. One small lesion (dotted arrow) is visible in measured b-values (mb1000 and mb1500) but not in the calculated b-values (cb1000 and cb1500) based on b = 100/800. In vcDWI, this small lesion is clearly visible if the calculation is based on b = 100/1000; In contrast, the lesion is masked if the calculation is based on b = 100/800.

contrast in computed high b-value images was at least 1.6 (cb1000) and 1.4 (cb1500), respectively, when an upper measured b-value of at least 800 s/mm^2 was chosen. For vcDWI, an upper b-value of 1000s/mm^2 should be preferred to maximize lesion SI and minimize CV resulting in a reliable lesion contrast of at least 2.1 in this study (besides the previously described case).

Our study has several limitations. Due to the small population size with different types of liver metastases we were only able to detect general trends and a potential area of application. Statistically significant differences could not be extracted since the signal in b-images is not a quantitative parameter and thus varies strongly between patients. On the other hand, our cohort represents a broad spectrum of

different kinds of metastatic liver lesions showing the general usability of the methods. The effectiveness of the different methods on specific diagnostic questions has to be investigated in future on dedicated clinical trials. The minimum diameter of included lesions was set to 1 cm to reduce partial volume effects for quantitative analysis. Therefore, the detectability of small lesions was not evaluated. Liver tissue without PET-positive lesions and other visible pathologies was defined as physiological; other diffuse inhomogeneities in liver parenchyma like small areas of fibrosis or steatosis which might have influence on diffusivity were not respected. Finally, the monoexponential fit is a simplified model which does not consider perfusion effects or other diffusion effects at high b-values, however, it is the most widely
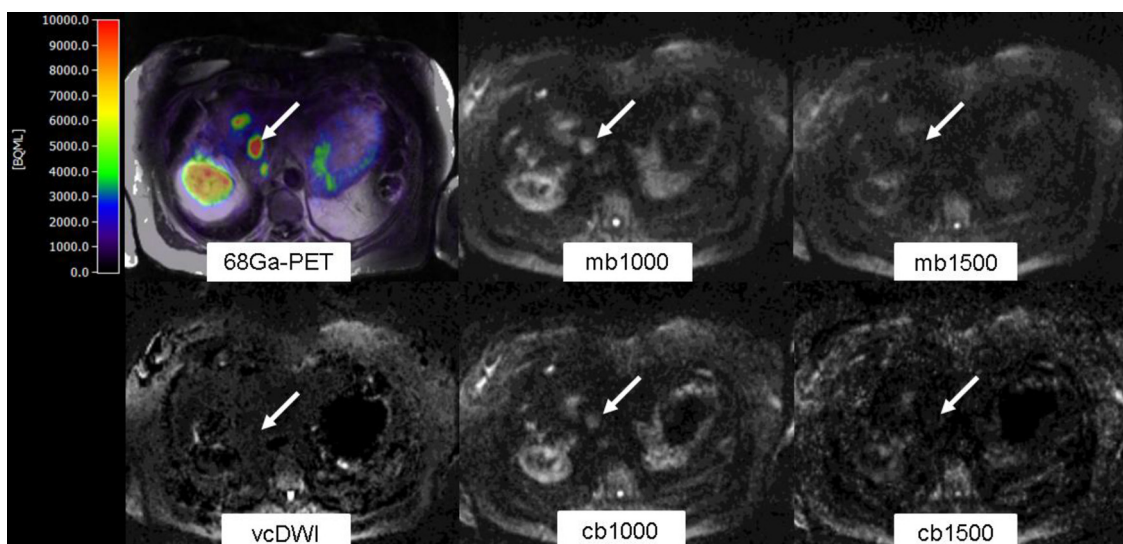
Fig. 6. Example of a 71 y/o female patient with 68Ga-PET-positive liver metastases of a neuroendocrine tumor. The patient had undergone a partial liver resection and chemotherapy. The lesion shows a distinct PET tracer uptake (top row, left hand side: PET overlaid with T2 TSE) which stands for a high expression of the somatostatin receptor (SSR). The lesion does not provide a considerable diffusion restriction which is a common finding in metastases of NET under therapy. Thus, the lesion is not distinguishable in b = 1500 images (mb1500/cb1500) or vcDWI. However, in b = 1000 images (mb1000/cb1000), the lesion is visible which can be explained by a T2-shine-through effect. All calculated b-values as well as the vcDWI were based on b = 100/800.

used approach in DWI allowing to quantify diffusion with only two b-value images.

In conclusion, we could show that the precision and the image characteristics of cDWI and vcDWI can be dependent on the selection of measured b-values the calculations are based on and in individual cases, the selection can have influence on the visibility of metastatic liver lesions. Higher measured upper b-values lead to more precise calculations of computed high b-value images with lower CVs. Based on our preliminary results, $b = 800\,s/mm^2$ as upper measured b-value seems therefore to be necessary to avoid misinterpretations in oncologic readings in the upper abdomen with cb1000 and cb1500, respectively. Adding additional lower b-value images to the monoexponential calculation seems not to improve the reliability of computed high b-value images, especially in the kidneys. vcDWI provides a comparable lesion contrast to $b = 1500s/mm^2$ images with higher signal intensities of lesions and offers additional features such as the reduction of T2 shine-through effects which could help to detect diffusion restricted liver lesions. However, caused by the underlying algorithm vcDWI is more susceptible to errors in the ADC-map; measuring $b = 1000s/mm^2$ as upper b-value seems therefore to be necessary to guarantee good lesion visibility in the liver.

Conflict of interest

The authors declare that they have no conflicts of interest.
Declarations of interest: none

Acknowledgements

References

[1] D.G. Norris, The effects of microscopic tissue parameters on the diffusion weighted magnetic resonance imaging experiment, NMR Biomed. 14 (2) (2001) 77–93.

[2] T. Ichikawa, H. Haradome, J. Hachiya, T. Nitatori, T. Araki, Diffusion-weighted MR imaging with a single-shot echoplanar sequence: detection and characterization of focal hepatic lesions, AJR Am. J. Roentgenol. 170 (2) (1998) 397–402.

[3] T. Yoshikawa, H. Kawamitsu, D.G. Mitchell, Y. Ohno, Y. Ku, Y. Seo, M. Fujii, K. Sugimura, ADC measurement of abdominal organs and lesions using parallel imaging technique, AJR Am. J. Roentgenol. 187 (6) (2006) 1521–1530.

[4] D.M. Koh, D.J. Collins, Diffusion-weighted MRI in the body: applications and challenges in oncology, AJR Am. J. Roentgenol. 188 (6) (2007) 1622–1635.

[5] A.R. Padhani, D.M. Koh, D.J. Collins, Whole-body diffusion-weighted MR imaging in cancer: current status and research directions, Radiology 261 (3) (2011) 700–718.

[6] E.O. Stejskal, J.E. Tanner, Spin diffusion measurements: spin echoes in the presence of a time-dependent field gradient, J. Chem. Phys. 42 (1) (1965) 288–292.

[7] K. Katahira, T. Takahara, T.C. Kwee, S. Oda, Y. Suzuki, S. Morishita, K. Kitani, Y. Hamada, M. Kitaoka, Y. Yamashita, Ultra-high-b-value diffusion-weighted MR imaging for the detection of prostate cancer: evaluation in 201 cases with histopathological correlation, Eur. Radiol. 21 (1) (2011) 188–196.

[8] M. Tozaki, E. Fukuma, 1H MR spectroscopy and diffusion-weighted imaging of the breast: are they useful tools for characterizing breast lesions before biopsy? AJR Am. J. Roentgenol. 193 (3) (2009) 840–849.

[9] L.K. Bittencourt, U.I. Attenberger, D. Lima, R. Strecker, A. de Oliveira, S.O. Schoenberg, E.L. Gasparetto, D. Hausmann, Feasibility study of computed vs measured high b-value (1400 s/mm(2)) diffusion-weighted MR images of the prostate, World J. Radiol. 6 (6) (2014) 374–380.

[10] M.C. Maas, J.J. Futterer, T.W. Scheenen, Quantitative evaluation of computed high B value diffusion-weighted magnetic resonance imaging of the prostate, Invest. Radiol. 48 (11) (2013) 779–786.

[11] M.D. Blackledge, M.O. Leach, D.J. Collins, D.M. Koh, Computed diffusion-weighted MR imaging may improve tumor detection, Radiology 261 (2) (2011) 573–581.

[12] K. Kitajima, Y. Kaji, K. Kuroda, K. Sugimura, High b-value diffusion-weighted imaging in normal and malignant peripheral zone tissue of the prostate: effect of signal-to-noise ratio, Magn. Reson. Med. Sci. 7 (2) (2008) 93–99.

[13] M. Vural, G. Ertas, A. Onay, O. Acar, T. Esen, Y. Saglican, H.P. Zengingonul, S. Akpek, Conspicuity of peripheral zone prostate cancer on computed diffusion-weighted imaging: comparison of cDWI1500, cDWI2000, and cDWI3000, Biomed Res. Int. 2014 (2014) 768291.

[14] S. Gatidis, H. Schmidt, P. Martirosian, K. Nikolaou, N.F. Schwenzer, Apparent diffusion coefficient-dependent voxelwise computed diffusion-weighted imaging: an approach for improving SNR and reducing T2 shine-through effects, J. Magn. Reson. Imaging 43 (4) (2016) 824–832.

[15] E.E. Sigmund, P.H. Vivier, D. Sui, N.A. Lamparello, K. Tantillo, A. Mikheev, H. Rusinek, J.S. Babb, P. Storey, V.S. Lee, H. Chandarana, Intravoxel incoherent motion and diffusion-tensor imaging in renal tissue under hydration and furosemide flow challenges, Radiology 263 (3) (2012) 758–769.

[16] S. Pazahr, D. Nanz, C. Rossi, N. Chuck, I. Stenger, M.C. Wurnig, F. Schick, A. Boss, Magnetic resonance imaging of the liver: apparent diffusion coefficients from multiexponential analysis of b values greater than 50 s/mm^2 do not respond to caloric intake despite increased portal-venous blood flow, Invest. Radiol. 49 (3) (2014) 138–146.

[17] R.V. Mulkern, A.S. Barnes, S.J. Haker, Y.P. Hung, F.J. Rybicki, S.E. Maier, C.M. Tempany, Biexponential characterization of prostate tissue water diffusion decay curves over an extended b-factor range, Magn. Reson. Imaging 24 (5) (2006) 563–568.

[18] A.B. Rosenkrantz, A.R. Padhani, T.L. Chenevert, D.M. Koh, F. De Keyzer, B. Taouli, D. Le Bihan, Body diffusion kurtosis imaging: basic principles, applications, and considerations for clinical practice, J. Magn. Reson. Imaging 42 (5) (2015) 1190–1202.

[19] F. Grinberg, E. Farrher, L. Ciobanu, F. Geffroy, D. Le Bihan, N.J. Shah, Non-Gaussian diffusion imaging for enhanced contrast of brain tissue affected by ischemic stroke, PLoS One 9 (2) (2014) e89225.

[20] H. Schmidt, S. Gatidis, N.F. Schwenzer, P. Martirosian, Impact of measurement parameters on apparent diffusion coefficient quantification in diffusion-weighted-magnetic resonance imaging, Invest. Radiol. 50 (1) (2015) 46–56.

[21] Y. Fukuda, I. Ohashi, K. Hanafusa, T. Nakagawa, S. Ohtani, Y. An-naka, T. Hayashi, H. Shibuya, Anisotropic diffusion in kidney: apparent diffusion coefficient measurements for clinical use, J. Magn. Reson. Imaging 11 (2) (2000) 156–160.

[22] G. Erbay, Z. Koc, E. Karadeli, B. Kuzgunbay, M.R. Goren, N. Bal, Evaluation of malignant and benign renal lesions using diffusion-weighted MRI with multiple b values, Acta Radiol. 53 (4) (2012) 359–365.

[23] R. Garcia-Carbonero, R. Garcia-Figueiras, A. Carmona-Bayonas, I. Sevilla, A. Teule, M. Quindos, E. Grande, J. Capdevila, J. Aller, J. Arbizu, P. Jimenez-Fonseca, Imaging approaches to assess the therapeutic response of gastroenteropancreatic neuroendocrine tumors (GEP-NETs): current perspectives and future trends of an exciting field in development, Cancer Metastasis Rev. 34 (4) (2015) 823–842.

[24] S.P. Li, A.R. Padhani, Tumor response assessments with diffusion and perfusion MRI, J. Magn. Reson. Imaging: JMRI 35 (4) (2012) 745–763.

[25] A.R. Padhani, D.M. Koh, Diffusion MR imaging for monitoring of treatment response, Magn. Reson. Imaging Clin. North Am. 19 (1) (2011) 181–209.

[26] E. Liapi, J.F. Geschwind, J.A. Vossen, M. Buijs, C.S. Georgiades, D.A. Bluemke, I.R. Kamel, Functional MRI evaluation of tumor response in patients with neuroendocrine hepatic metastasis treated with transcatheter arterial chemoembolization, AJR Am. J. Roentgenol. 190 (1) (2008) 67–73.